Influence of Preload on Failure Modes of Hybrid Metal-Composite Protruding Bolted Joints

Calin-Dumitru COMAN*

*Corresponding author
INCAS – National Institute for Aerospace Research "Elie Carafoli",
B-dul Iuliu Maniu 220, Bucharest 061126, Romania,
coman.calin@incas.ro

DOI: 10.13111/2066-8201.2021.13.1.4

Received: 11 December 2020/ Accepted: 12 January 2021/ Published: March 2021

International Conference of Aerospace Sciences "AEROSPATIAL 2020", Virtual Conference
15-16 October 2020, Bucharest, Romania,
Section 4 - Materials and Structures

Abstract: *This paper presents the effects of torque preload on the damage initiation and growth in the CFRP (Carbon Fiber Reinforced Polymer) composite laminated adherent of the single-lap, single-bolt, hybrid metal-composite joints. A detailed 3D finite element model incorporating geometric, material and friction-based contact full nonlinearities is developed to numerically investigate the preload effects on the progressive damage analysis (PDA) of the orthotropic material model. The PDA material model integrates the nonlinear shear response, Hashin-tape failure criteria and strain-based continuum elastic properties degradation laws being developed using the UMAT user subroutine in Nastran commercial software. In order to validate the preload effects on the failure modes of the joints with hexagonal head bolts, experiments were conducted using the SHM (Structural Health Monitoring) technique. The results showed that the adherent torque level is an important parameter in the design process of an adequate bolted joint and its effects on damage initiation and failure modes were quite accurately predicted by the PDA material model, which proved to be computational efficient and can predict failure propagation and damage mechanism in hybrid metal-composite bolted joints.*

Key Words: *Hybrid bolted joints, progressive damage analysis, finite element analysis, bolt preload, failure modes.*

1. INTRODUCTION

The aerospace industry became the most common application field for fiber-reinforced polymer matrix composites (PMCs) due to their lightweight properties [1]. These structural components are often assembled in conjunction with metal parts using mechanically fastened joints, resulting in hybrid metal-composite joints that cause some challenging problems for mechanical engineers. Poorly designed hybrid joints is not only a source of failure, but could lead to a reduction in durability and reliability of the whole structure. Up to nowadays, the researchers studied the failure analysis of composite bolted joints using a method that combines continuum damage mechanics (CDM) [2] with finite element analysis (FEA). In the CDM models, the local damage onset appears at a low values of applied load and damage accumulation is developed with increasing load according to damage propagation laws, which

makes the method accurate and able to predict various failure modes. The major disadvantage of the CDM models is the huge amount of test data required for model calibrations. The progressive damage analysis (PDA) in composite materials, which is based on the stress-strain law, showed that the material orthotropic properties reduction due to damage initiation is essential for the stress field analysis [3-7]. A lot of PDA models in research field [8-11] incorporated shear nonlinearity, Hashin-type failure criterion and constant elastic properties degradation low for orthotropic materials, which makes the method quite easy to implement and computational efficient. Because these properties degradation models used constant factors for elastic properties reduction due to damage growth, the models weren't be able to predict the bearing final failure. Models containing continuous degradation rules started to appear in the literature [12], [13] to improve the numeric algorithm efficiency and to obtain a smoother loading-displacement curve. A major shortcoming of these models is that they focused only on a few types of failure modes and not on various joint failure modes. The composite progressive damage behavior is a complex nonlinear phenomenon and in conjunction with geometric and contact nonlinearities can lead to convergence issues of the finite element method (FEM) analysis, mostly in implicit numerical algorithms which implies that a lot of effort is concentrating for obtaining a better solution toward to ultimate global structure failure [14]. The difficulties arising from composite material usage on structural failure analysis, are that these materials have anisotropic mechanical properties, brittle and low inter-laminar strength [15]. This study describes and develops a progressive damage analysis using an adequate material model for composite adherent that can predict the bolt preload effects on structural behavior and failure modes of hybrid metal-composite bolted joints. It takes into account all the nonlinearities phenomena involved in the load distribution through the joint as the geometric nonlinearity which implies large deformations, friction based nonlinear contact and material nonlinearities due to shear deformations of the lamina, Hashin-type failure criterion and strain-based continuous degradation law implemented using an user subroutine coded in Fortran programming language and commercial Nastran SOL 400 solver. A series of experiments were conducted in order to validate the FE model and PDA results involving the influence of bolt preload on the failure modes of the hybrid-metal composite joints. The experimental and numerical results were quite accurate.

2. PROBLEM DESCRIPTION

- Joint geometry description

Single-lap joints (SLJ) with single hexagonal head bolt were manufactured using both metal and composite materials for the adherents. The geometry design parameters were chosen in accordance with ASTM standard [16] to induce bearing failure. The in plane dimensions of the adherents are presented in Table 1 and Fig. 1. The adherent thicknesses are different, 4 mm for the metal adherent and 3 mm for the laminated adherent. Hexagonal head stainless steel bolts with nominal diameter of 5 mm were used. The applied torque levels to the bolt shank are presented in Table 1.

The composite adherent was manufactured of carbon-epoxy pre-pregs with fiber volume fraction of 32%. The stacking sequence is as follows [0/90/0/90/0/90] using 0.33 mm thickness unidirectional lamina, with the elastic properties presented in Table 2.

The metal adherent was manufactured of aluminum alloy AA 7075T6 [17] and the bolts, nuts and washers were made of stainless steel A2-70 [17] with the elastic properties presented also in Table 2.

Table 1. Experiment set-up

Length [mm]	Width [mm]	e [mm]	Torque [Nm]	Temperature [^oC]
150	34	10	0.5/2/3/4/5	+50

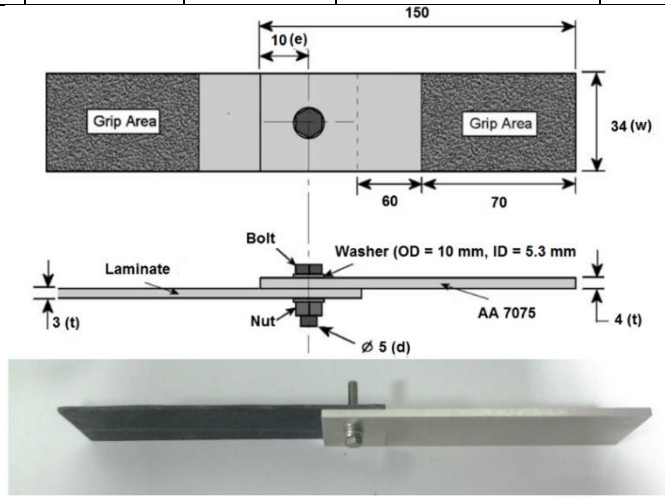

Figure 1. Joint geometry, dimensions in mm

Table 2. Mechanical properties of the materials

Property	CFRP Lamina	AA 7075T6 [17]	A2-70 [17]
Longitudinal modulus E_{11} [MPa]	34433	71016	206000
Transversal modulus E_{22} [MPa]	3610		
Through-thickness modulus, E_{33} [MPa]	3610		
Shear modulus G_{12} [MPa]	2421	26890	75842
Shear modulus G_{23} [MPa]	2421		
Shear modulus G_{13} [MPa]	1561		
Poisson coefficient ν_{12}	0.36	0.33	0.36
Poisson coefficient ν_{23}	0.45		
Poisson coefficient ν_{13}	0.35		
Longitudinal tensile strength $\sigma_{11,\,max}^{T}$, [MPa]	253		
Longitudinal compression strength $\sigma_{11,\,max}^{C}$, [MPa]	230		
Transversal compression strength $\sigma_{22,\,max}^{C}$, [MPa]	74		
In plane shear strength τ_{12}^{max}, [MPa]	25		
Out plane shear strength τ_{23}^{max}, [MPa]	37		
Out plane shear strength τ_{13}^{max}, [MPa]	37		

Note: (1, 2, 3) are the lamina on-axis coordinate system.

The unidirectional lamina properties presented in Table 2 were obtained using ASTM [18]-[20] standards on the unidirectional laminated specimens. The bearing tests were conducted in accordance with ASTM standard [16]: the specimens were gripped into a 30 kN Instron testing machine, the torque level was applied to the bolt shank and then the displacement controlled tensile loading of 0.3 mm/min was applied until ultimate failure. The experiment set-up is shown in Fig. 2.

- Numerical analysis

A tridimensional finite element model, using linear brick elements, was developed in commercial software MSC Patran, as shown in Fig. 3. Each separate part was modeled: metal

and composite adherents, the washer and a combined bolt-nut part. The adherents were modeled with high radial mesh density around the hole, where there are high strain gradients exist. Thus, the minimum element length is 0.33 mm around the hole. The minimum element length is increasing up to 1 mm from hole towards the clamped ends of the adherents. In order to avoid rigid body motions, light springs were attached to the components not fully constrained, such as the bolt, washer and laminate adherent. For simulating the bolt pre-load due to the torque level, it was used a dedicated Bolt Preload module in Patran. This is done by sectioning the bolt shank in the shear plane location which separates the shank in two parts and creates coincident nodes at the interface cutting plane. These coincident nodes are then connected by an over-closure MPC (Multi Points Constrain) and loaded with axial preload.

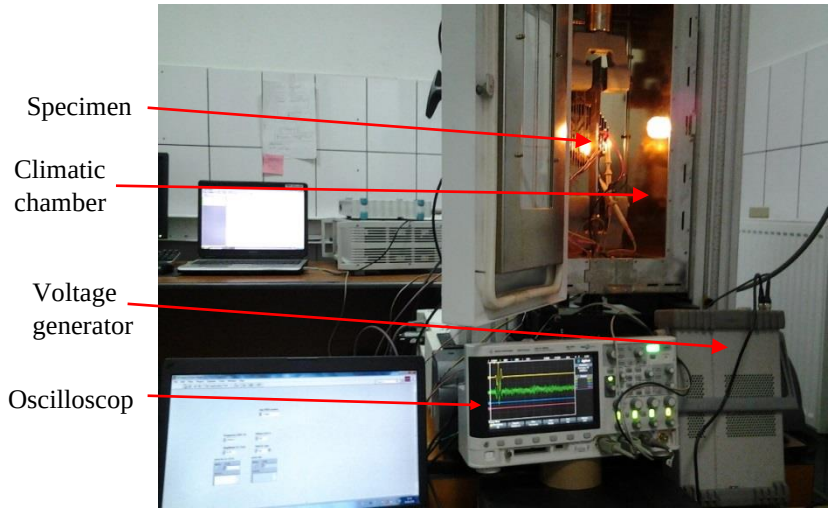

Figure 2. Experimental workbench

Regarding the clamping of the joint in the test machine, the boundary conditions imposed on the numerical model are presented in Fig. 3. They represent the fixing of all translations only on the upper and lower surfaces of the leftmost end of the metal adherent and only the suppression of the translations in the y and z directions, imposing a prescribed displacement in the x direction at the rightmost end of the composite adherent.

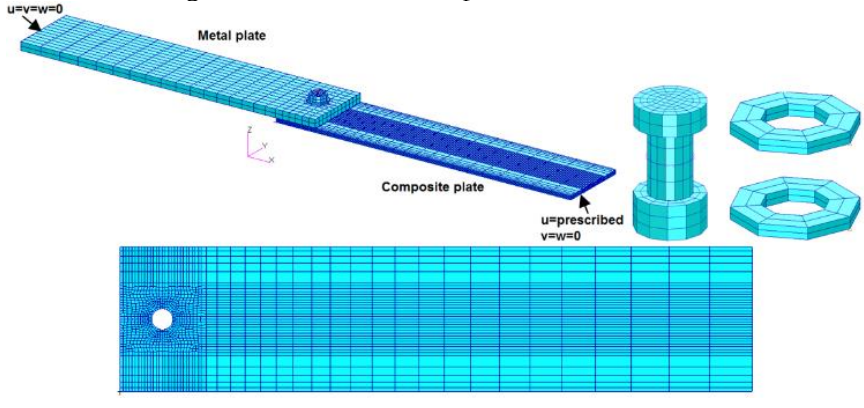

Figure 3. Finite element model and boundary conditions

The laminated adherent is modeled with continuum solid-shell special elements available in MSC. Nastran 2012. These special solid elements have bending properties like shells and one integrating point per element. The finite element model has six elements per laminate

thickness, with one solid-shell element per each ply, thus, stress in each ply can be determined and the correct bending-twisting coupling is obtained. All metallic parts are modelled with continuum solid elements with large strain property assumed. In the 3D model, the contact between the bolt and the surface of the hole is achieved by the direct method of the constraints explained in the following.

The method requires the definition of contact bodies, solids that can be in contact. The bodies in contact may be whole physical solids (laminated adherents, bolt, washer), but it has been shown [21] that it is more efficient to consider sets of elements of these physical bodies in contact, as shown in Fig. 4, because the number of checks for contact between bodies at each iteration of the solution is reduced.

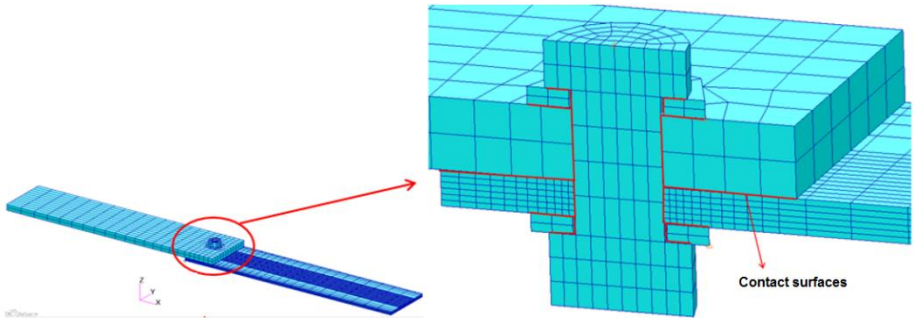

Figure 4. Contact elements in 3D model

Another step in defining nonlinear contact phenomenon is the choice between the analytical and the discreet contact, which will be briefly described below. When a node on a solid reaches the contact segment on the other solid, the node is constraint on this segment along the normal to this segment. In the case of discrete contact for normal detection, the linear representation with the finite elements of the contact surface is used which leads to the calculation of the normal of each element. If the surface is not planar, when the node touching the contact segment on the surface of the other solid in contact, being in the tolerated contact area, it is shifted and constrained on the contact segment, making possible the moving process and constraint**;** the surface having a curve, the node locks between two differently normal elements due to the discontinuity of the normal elements. This impediment has an adverse effect on the quality of the results as observed by McCarthy et al. [21] in their work on single bolt joint, single shear of composite materials. In the case of analytical contact, a smooth Coons surface is constructed through the nodes of the solid contact segment, and then this analytical surface is used to calculate the continuous normal at the contact surface between the two solids, thus solving the problem of node blocking due to the discontinuity of normal the contact surface between the bodies. This method leads to a better representation of the geometry of the joint, especially its deformation and the accuracy of the numerical results is far superior to the technique of discrete contact [21].

3. BOLT PRELOAD EFFECTS ON THE JOINT FAILURE

- SHM method description

A common and useful method for structure health monitoring (SHM) is using the guided waves. The major advantage of these waves is the low energy losing while passing through the structure, which denotes an excellent energy transfer through the entire structure. The pioneer of this method is Horace Lamb who first published his result for the first time in 1917

[22]. There are two types of propagation modes for these waves: symmetric mode (S_0, $S_1 \ldots S_n$) and anti-symmetric (A_0, $A_1, \ldots, A_n$) [23]. In many applications, the most used modes for SHM testing are the fundamental mode S_0, which is dominating at 150-300 Hz and A_0 at 30-100 Hz frequencies. The reason for choosing these two fundamental modes is that they are easier to identify from the oscillation group of modes than the other superior ones. The SHM testing technique was used to experimentally observe the first ply failure in the laminate adherent.

The PWAS devices used in this experiment are produced by STEMiNC company, having the part number SMPL7W7T02412. They have a circular shape with 5 mm diameter and are presented in Fig. 5. The input signal is a sinusoidal tone burst type signal having 20 V peak to peak amplitude with Hanning window amplitude modulation. This signal includes 3 periods and is generated by an Agilent 33120 signal generator.

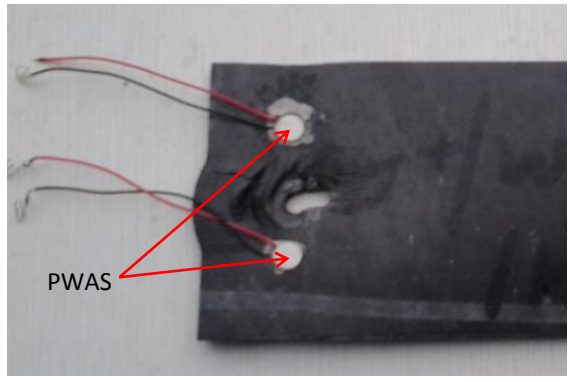

Figure 5. PWAS positions on composite adherent

Fig. 6 presents the damage initiation effect on the amplitude of the received signal and force-displacement characteristic curve, in order to be able to identify the first ply failure of the laminated adherent of the joint. The amplitude curves represent the maximum (peak to peak) amplitudes of each receiving signals during the test. During a test the input and output signals of the two PWAS's from the laminated adherent are acquisitioned with a period of 2 seconds. From Fig. 6 it can be clearly seen that the amplitude of output signal is increasing while the joint is stiffening up to the first lamina failure event. Afterwards the amplitude is decreasing due to the elastic properties degradation in the laminate adherent on the post failure stage. As a conclusion, it can be considered that SHM method accurately predicts the first ply failure and joint limit load which represents the fiber compression damage at the lamina level, because this local damage corresponds to a significant decreasing of the joint stiffness.

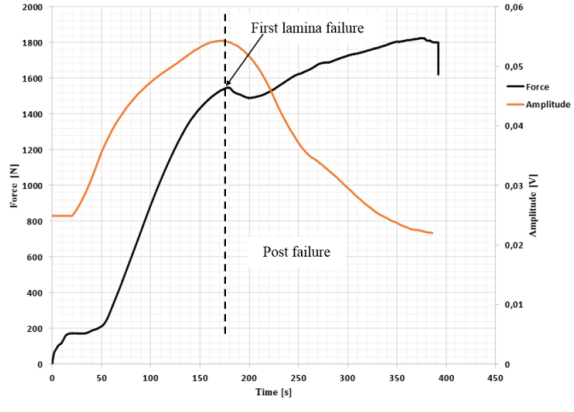

Figure 6. Damage effects on output signal, bolt torque 0.5 Nm

- Nonlinear shear deformation

The simulation must take into account the two most important nonlinear mechanisms: lamina nonlinear shear deformations and stiffness reduction due to damage accumulation at lamina level. These two nonlinearities are taken into account using an external user-defined subroutine named USER_MAT, edited in FORTAN language. USER_MAT calls the modified Nastran material user-defined subroutine UMAT, in order to implement the material nonlinearities specified above. Hahn and Tsai developed [24] the in plane nonlinear shear lamina constitutive model using high order elasticity theory:

$$\gamma_{12} = \frac{\tau_{12}}{G_{12}} + \beta \cdot \tau_{12}^3 \tag{1}$$

where β is a material parameter that can be determined by experiments only. Fig. 7 shows the experimental curve of the shear deformation γ_{12} as a function of the shear stress τ_{12} obtained using off-axis tension tests on unidirectional laminate. From Fig. 7, by polynomial interpolation, it was obtained the coefficient $\beta = 0.635$ (MPa)$^{-3}$ for this type of lamina used in the study. This constitutive relation can be implemented in USER_MAT user subroutine as it is described in [25]:

$$\tau_{12}^{(t+\Delta t)} = \frac{1+2\cdot\beta\cdot(\tau_{12}^t)^3\cdot(\gamma_{12}^t)^{-1}}{1+3\cdot\beta\cdot {G_{12}}^0\cdot(\tau_{12}^{(i)})^2}\cdot {G_{12}}^0\cdot\gamma_{12}^{t+\Delta t} \tag{2}$$

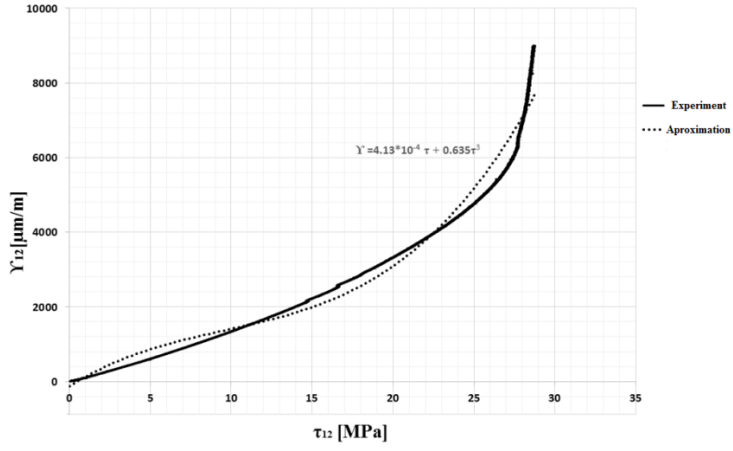

Figure 7. Nonlinear shear–strain experimental curve

The orthotropic stress-strain constitutive relationship is given by equations (3) and (4), according to [25]:

$$\begin{bmatrix}\sigma_{11}^{t+\Delta t}\\ \sigma_{22}^{t+\Delta t}\\ \sigma_{33}^{t+\Delta t}\end{bmatrix} = \begin{bmatrix} E_{11}B(1-\vartheta_{23}\vartheta_{32}) & E_{22}B(\vartheta_{12}-\vartheta_{13}\vartheta_{32}) & E_{33}B(\vartheta_{13}-\vartheta_{12}\vartheta_{23}) \\ E_{22}B(\vartheta_{12}-\vartheta_{13}\vartheta_{32}) & E_{22}B(1-\vartheta_{13}\vartheta_{31}) & E_{22}B(\vartheta_{32}-\vartheta_{12}\vartheta_{31}) \\ E_{33}B(\vartheta_{13}-\vartheta_{12}\vartheta_{23}) & E_{22}B(\vartheta_{32}-\vartheta_{12}\vartheta_{31}) & E_{33}B(1-\vartheta_{12}\vartheta_{21}) \end{bmatrix} \times \begin{bmatrix}\varepsilon_{11}^{t+\Delta t}\\ \varepsilon_{22}^{t+\Delta t}\\ \varepsilon_{33}^{t+\Delta t}\end{bmatrix} \tag{3}$$

$$\begin{bmatrix}\tau_{12}^{t+\Delta t}\\ \tau_{23}^{t+\Delta t}\\ \tau_{31}^{t+\Delta t}\end{bmatrix} = \begin{bmatrix} Rel.(6) & 0 & 0 \\ 0 & G_{23} & 0 \\ 0 & 0 & G_{31} \end{bmatrix} \times \begin{bmatrix}\gamma_{12}^{t+\Delta t}\\ \gamma_{23}^{t+\Delta t}\\ \gamma_{31}^{t+\Delta t}\end{bmatrix} \tag{4}$$

where:

$$B=\frac{1}{1-\vartheta_{12}\vartheta_{21}-\vartheta_{23}\vartheta_{32}-\vartheta_{13}\vartheta_{31}-2\cdot\vartheta_{21}\vartheta_{32}\vartheta_{13}} \tag{5}$$

$$\tau_{12}^{t+\Delta t}=\begin{cases}\dfrac{1+2\cdot\beta\cdot(\tau_{12}^{t})^{3}\cdot(\gamma_{12}^{t})^{-1}}{1+3\cdot\beta\cdot {G_{12}}^{0}\cdot(\tau_{12}^{t})^{2}}\cdot {G_{12}}^{0}\cdot\gamma_{12}^{(t+\Delta t)}, & FI=0\\ {G_{12}}^{t+\Delta t}\cdot\gamma_{12}^{t+\Delta t}, & FI\geq 1 \text{ and } {G_{12}}^{t+\Delta t}\cdot\gamma_{12}^{t+\Delta t}<\tau_{12}^{init}\\ \tau_{12}^{init}, & FI\geq 1 \text{ and } {G_{12}}^{t+\Delta t}\cdot\gamma_{12}^{t+\Delta t}\geq\tau_{12}^{init}\end{cases} \tag{6}$$

$$FI=max\,(FI_{1},\,FI_{2}) \tag{7}$$

In relation (6), G_{12}^0 is the initial in-plane shear modulus which is reduced according to degradation rules specified in relation (11), once fiber compression-shear failure happened. The shear stress τ_{12}^{init} is a threshold used to avoid any over-estimation of the shear stress after any failure that can reduce the shear modulus G_{12}.

- Failure criteria and continuous degradation rules

The most dominant micro-failure modes for bearing joints are matrix compression and fiber shear-compression failures, so an important attention is paid to them in this failure study. For the PDA of the laminated plate around the hole, Hashin [26] failure criteria are used and the failure indexes are calculated using relation (8) for matrix compression failure and relation (9) for fiber compression and matrix-fiber shear failure:

$$FI_1=\left[\left(\frac{\sigma^{C}_{22,\,max}}{2\cdot\tau_{23}^{max}}\right)^{2}-1\right]\cdot\frac{\sigma_2+\sigma_3}{\sigma^{C}_{22,\,max}}+\frac{(\sigma_2+\sigma_3)^2}{4\cdot(\tau_{23}^{max})^2}-\frac{\sigma_2\cdot\sigma_3}{(\tau_{23}^{max})^2}+\left(\frac{\tau_{12}}{\tau_{12}^{max}}\right)^{2}+\left(\frac{\tau_{13}}{\tau_{13}^{max}}\right)^{2}+\left(\frac{\tau_{23}}{\tau_{23}^{max}}\right)^{2}+\left(\frac{\sigma_1}{\sigma^{T}_{11,\,max}}\right)^{2} \tag{8}$$

$$FI_2=\left(\frac{\sigma_1}{\sigma^{C}_{11,\,max}}\right)^{2}+\left(\frac{\tau_{12}}{\tau_{12}^{max}}\right)^{2}+\left(\frac{\tau_{13}}{\tau_{13}^{max}}\right)^{2} \tag{9}$$

- Continuous degradation rules for elastic moduli

A strain based degradation rule is proposed for reduction of E_{ii} (i=1…3) as described in [27]. The fiber or matrix failure initiate at a user-defined failure strain $\varepsilon_{ii}^{\text{init}}$ and PDA stiffness reductions are performed using [27]:

$$E_{ii}^{t+\Delta t}=\begin{cases}E_{ii}^{0}\cdot\left(1-d_i\cdot\dfrac{\varepsilon_{ii}^{t+\Delta t}-\varepsilon_{ii}^{init}}{\Delta\varepsilon_{ii}}\right), & \varepsilon_{ii}^{init}\leq\varepsilon_{ii}^{t+\Delta t}<\varepsilon_{ii}^{init}+\Delta\varepsilon_{ii}\\ E_{ii}^{0}\cdot(1-d_i)\dfrac{\varepsilon_{ii}^{init}+\Delta\varepsilon_{ii}}{\varepsilon_{ii}^{t+\Delta t}}, & \varepsilon_{ii}^{t+\Delta t}\geq\varepsilon_{ii}^{init}+\Delta\varepsilon_{ii}\end{cases} \tag{10}$$

where E_{ii}^0 is the initial modulus of elasticity from Table 2 for lamina orthotropic directions, $\Delta\varepsilon_{ii}$ is a user-defined strain step to ensure a smooth reduction of the properties upon failure and d_i is the reduction factor. Initial failure strain and corresponding stress ε_{ii}^{init}, σ_{ii}^{init} are determined by simulation for FI=1 according to relation (7). The reduction parameters for E_{ii} (i=1… 3) are presented in Table 3 and obtained after several parameter tuning iterations.

Table 3. Degradation parameters for elastic moduli

Failure mode	d_i	$\Delta\varepsilon_{ii}$
Fiber shear-compression (i=1)	0.6	0.005
Matrix compression (i=2, 3)	0.8	0.005

- Continuous degradation rules for shear moduli

The in-plane shear modulus G_{12} is continuous reduced using the shear strain $\gamma_{ij}^{t+\Delta t}$ for $FI > 1$, according to [27]:

$$G_{ij}=G_{ij}^{0}\left(0.1+0.9\cdot\frac{\gamma_{ij}^{init}}{\gamma_{ij}^{t+\Delta t}}\right),\ i\neq j=1\ldots3 \tag{11}$$

- Poisson's coefficient reduction

In [28] a continuous reduction of the Poisson's ratio is proposed in order to comply with elastic stability of the orthotropic materials:

$$\vartheta_{12}=\vartheta_{12}^{0}\cdot\sqrt{\frac{E_1E_2^0}{E_2E_1^0}}\ ,\ \vartheta_{13}=\vartheta_{13}^{0}\cdot\sqrt{\frac{E_1E_3^0}{E_3E_1^0}}\ ,\ \vartheta_{23}=\vartheta_{23}^{0}\cdot\sqrt{\frac{E_2E_3^0}{E_3E_2^0}} \tag{12}$$

4. RESULTS AND DISCUSSIONS

In order to better understand the nonlinear structural behavior and failure mechanisms of the joint, the load-displacement curves are presented in Fig. 8.

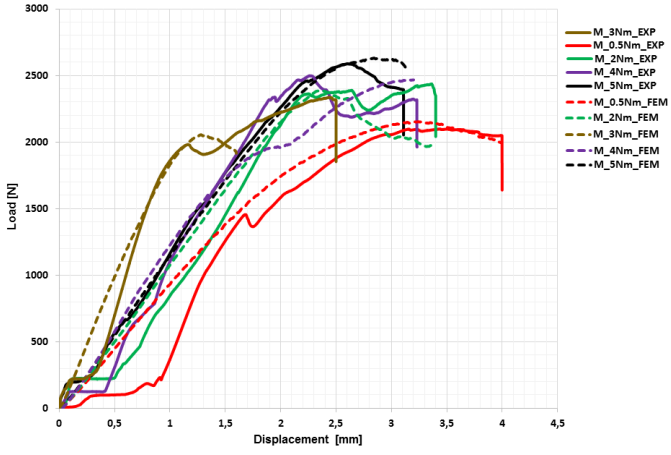

Figure 8. Experimental and numerical load-displacement curves

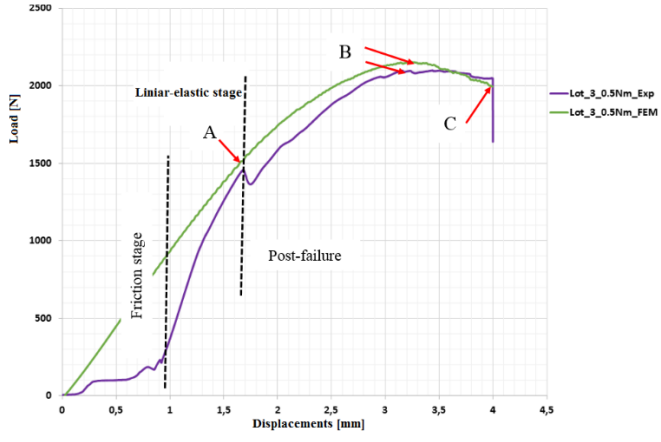

Figure 9. Load-displacement curve, 0.5 Nm

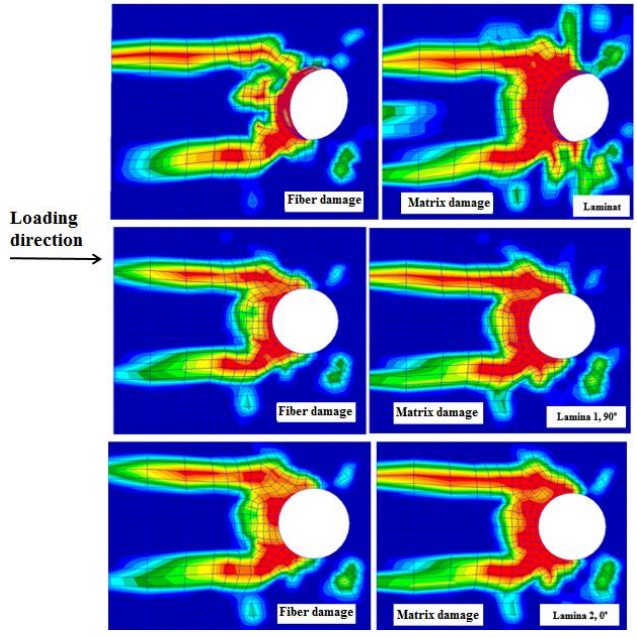

Figure 10. Progressive failure, point C, 0.5 Nm

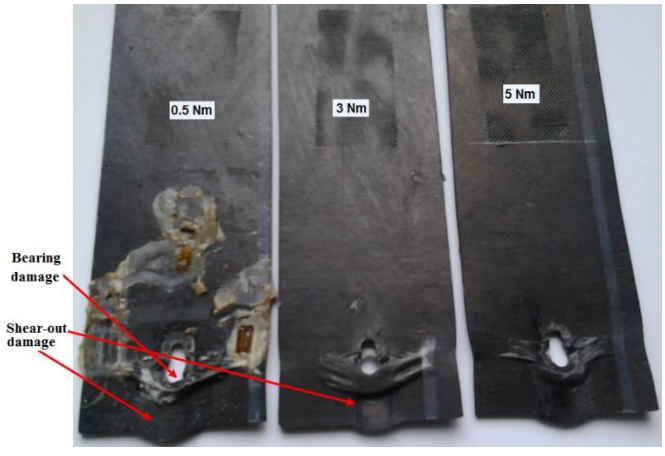

Figure 11. Composite failure modes

The comparison between experimental and numerical results in terms of bolt preload effects on damage initiation and progressive failure mechanisms are presented in the following. Load-displacement curve for 0.5 Nm torque level is presented in Fig. 9. Simulation and experiment results regarding progressive failure around the hole in the laminated adherent are presented in Figs. 10-11. At the beginning of the experimental force-displacements curve it is observed a nonlinear behavior due to friction between the adherents. Increasing the applied tensile load up to approximately 255 N, the adherents will not move relative to each other, due to static friction between them and the forces are transmitted only by friction. Point A represents the first damage initiation point in laminate adherent, denoting the limit load of the joint and is located on the graph at the major deviation of the force-displacements curves from linear behavior.

At this point, the compression fibers damage appears first as an indicator of the bearing failure initiation, despite the appearance of the fiber-matrix shear damage which is observed

also in point A. Matrix compression damage is also present at point A, but this does not contribute a lot to the joint stiffness decrease, because fibers have the most important role in joint stiffening, but not the matrix.

In Fig. 9, point B represents the joint ultimate failure. After the point A, the damage accumulation determines joint stiffness reduction gradually and the characteristic curve becomes nonlinear. From point A up to point B, the post failure stage is completely developed, where the residual stiffness is continuously reduced. On this stage, the fiber compression, matrix compression and fiber-matrix shear damage are increasing at the bearing plane through the whole thickness of the laminate adherent. Point C represents the catastrophic final failure of the joint, when fiber compression, matrix compression and fiber-matrix shear damages start and propagate on approximately +/- 45° from loading direction and are extended to a large portion of the laminate adherent on the bearing plane through free edge behind the hole of the laminate, as can easily be seen from Fig. 10.

As can be seen from Fig. 10, in 0° plies the fibers damage is greater than the matrix damage, while in 90° plies the two micro level damages have almost the same spread out. In Fig. 10, the dark blue color represents undamaged elements, while the red color states for E^0_{ii} $(1-d_i)$ residual stiffness of the elements. From Fig. 10 it can be observed that the most damaged layer is located on the top surface of the laminate, considering that the laminate adherent was modeled with only one element per each ply in the thickness direction. The position of the first ply failure could be affected by the bolt tilting in the hole due to the exiting joint clearance and secondary bending effect.

A summary of the bolt preload effects on the progressive failure of the metal-composite hybrid joints is presented in Table 4 and Fig. 12. In Table 4, $F_{L.L}$ and $F_{U.L}$ represent the limit and ultimate forces of the joint to axial quasi-static tensile loading, corresponding to the A and B points from the characteristic force-displacements curves as discussed above.

Table 4. Bolt torque effect on joint strength

M [Nm]	$F_{L.L}$ [N]		$F_{U.L}$ [N]	
	EXP.	FEM	EXP.	FEM
0.5	1447.37	1500.03	2175.83	2153.89
2	1960.15	2025.22	2436.18	2385.31
3	1978.69	1950.52	2561.98	2552.97
4	2305.15	2280.59	2497.64	2470.22
5	2446.33	2394.58	2557.81	2530.38

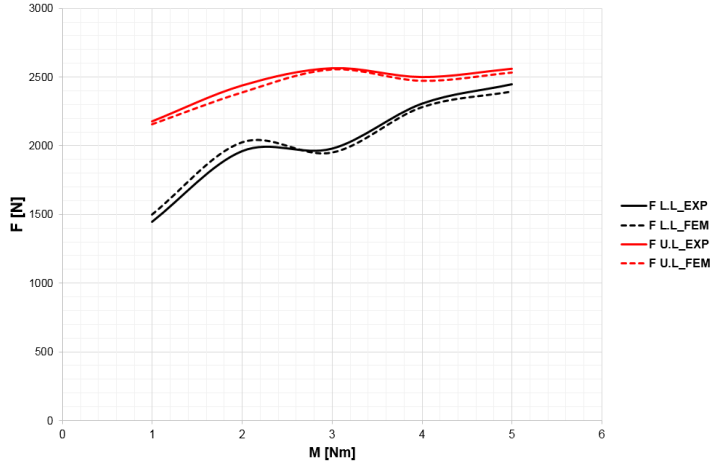

Figure 12. Preload torque effects on the force capacity of the joint

5. CONCLUSIONS

In this paper, the bolt preload effects on the damage initiation and progressive failure of single-lap, single-bolt, hybrid metal-composite joints are investigated using both SHM (Structural Health Monitoring) experimental technique and simulations with finite element method (FEM). Regarding the first ply failure (FPF) and strength evaluations, a progressive damage analysis (PDA) including nonlinear shear behavior of the ply, Hashin-type failure criteria and strain-based continuous degradation laws were proposed. A 3D FEM model, which incorporates geometrical, material and contact full nonlinearities was developed in Patran as preprocessor and Nastran as explicit iterative solver. The PDA material model was implemented using a user-defined subroutine namely User_mat, using FOTRAN programming language.

The simulation results were in good agreement with the experiments in terms of load-displacement behavior, FPF and ultimate failure loads, which denoted that the 3D FEM model including full nonlinearities and explicit solver are quite accurate and can predict the metal-composite joint's mechanical behavior on both linear-elastic and nonlinear elastic ranges, including the failure modes as bearing and shear-out. Regarding the bolt preload effects on the load-displacement curves, Fig. 8 shows that the bolt torque levels increase the axial stiffness of the joint, but have no major effect on the joint ultimate load, (see Table 4 and Fig 12). Regarding the FPF and strength predictions, the SHM technique proved to be quite accurate in evaluating the damage initiation and accumulation until the final failure.

ACKNOWLEDGEMENTS

Funding: This work was supported by the EU Structural Funding through "Be Antreprenor!" Project [grant number 51680/09.07.2019POCU/380/6/13-SMIS code: 124539], under the consideration of The "Politehnica" University of Bucharest.

REFERENCES

[1] Y. Xiao, T. Ishikawa, Bearing strength and failure behavior of bolted composite joints (part II: modeling and simulation), *Compos. Sci. and Technol.*, **65**, 1032–1043, 2005.
[2] J. L. Chaboche, Continuum damage mechanics: part I – General concepts; part II – damage growth, crack initiation and crack growth, *J. of App. Mech.*, **55**, 59–72, 1988.
[3] F. K. Chang, K. Y. Chang, Post-failure analysis of bolted composite joints in tension or shear-out mode failure, *J. of Compos. Mat.*, **21**, 809–833, 1987.
[4] L. B. Lessard, M. M. Shokrieh, Two-dimensional modeling of composite pinned-joint failure, *J. of Compos. Mat.*, **29**, 671–697, 1995.
[5] C. L. Hung, F. K. Chang, Bearing failure of bolted composite joints. Part II: model and verification, J. *of Compos. Mat.*, **30**, 1359–1400, 1996.
[6] S. J. Kim, J. S. Hwang, J. H. Kim, Progressive failure analysis of pin-loaded laminated composites using penalty finite element method, *J. AIAA*, **36**, 75–80, 1998.
[7] P. P. Camanho, F. L. Matthews, A progressive damage model for mechanically fastened joints in composite laminates, *J. of Compos. Mat.*, **33**, 2248–2280, 1999.
[8] B. Okutan, The effects of geometric parameters on the failure strength for pin-loaded multi-directional fiber-glass reinforced epoxy laminate, *Compos. Part B-Eng.*, **33**, 567–568, 2002.
[9] K. I. Tserpes, G. Labeas, P. Papanikos, Th. Kermanidis, Strength prediction of bolted joints in graphite/epoxy composite laminates, *Compos. Part B-Eng.*, **33**, 521–529, 2002.
[10] Á. Olmedo, C. Santiuste, On the prediction of bolted single-lap composite joints, *Compos. Struct.*, **94**, 2110–2117, 2012.
[11] Z. Kapidz˘ic´, L. Nilsson, H. Ansell, Finite element modeling of mechanically fastened composite-aluminum joints in aircraft structures, *Compos. Struct.*, **109**, 198–210, 2014.

[12] A. K. Zerbst, G. Kuhlmann, C. Steenbock, et al., Progressive damage analysis of composite bolted joints with liquid shim layers using constant and continuous degradation models, *Compos. Struct.*, **92**, 189–200, 2010.
[13] G. Kolks, KI. Tserpes. Efficient progressive damage modeling of hybrid composite/ titanium bolted joints, *Compos. Part A-Appl. S. and Manuf.*, **56**, 51–63, 2014.
[14] B. Egan, M. A. McCarthy, R. M. Frizzell, P. J. Gray, C. T. McCarthy, Modelling bearing failure in countersunk composite joints under quasi-static loading using 3D explicit finite element analysis, *Compos. Struct.*, **108**, 963–977, 2014.
[15] Á. Olmedo, C. Santiuste, E. Barbero, An analytical model for the secondary bending prediction in single-lap composite bolted-joints, Compos. Struct., **111**, 354–361, 2014.
[16] * * * *ASTM D 5961, Standard test method for bearing response of polymer matrix composite laminates*, ASTM Int., 2007.
[17] * * * *MMPDS-05, Metallic Materials Properties development and Standardization*, FAA, 2010.
[18] * * * *ASTM D 3039, Standard Test Method for Tensile Properties of Polymer Matrix Composite Materials*, ASTM Int., 2007.
[19] * * * *ASTM D 5379, Standard Test Method for Shear Propeties of Composite Materials by the V-Notched Beam Method*, ASTM Int, 2008.
[20] * * * *ASTM D 3410, Standard Test Method for Compressive Properties of Polymer Matrix Composite Materials*, ASTM Int, 2007.
[21] M. A. McCarthy, C. T. McCarthy, V. P. Lawlor, W. F. Stanley, Three-dimensional finite element analysis of single-bolt, single-lap composite bolted joints: part I - model development and validation, *Compos. Struct.*, **71**, 140-158, 2004.
[22] H. Lamb, On Waves in an Elastic Adherent, *Proc. of the Royal Society, Math. Phy. and Eng. Sci.*, **93**, 114 – 128, 1917.
[23] V. Giurgiutiu, J. Bao, Embedded Ultrasonic Structural Radar with Piezoelectric Wafer Active Sensors for the NDE of Thin-Wall Structures, *Proc. ASME Int. Mech. Eng. Congress*, New Orleans, USA, 2002.
[24] H. T. Hahn, S. W. Tsai, Nonlinear elastic behavior of unidirectional composite laminates, *J. of Compos. Mater.*, **7**, 102–18, 1973.
[25] A. Du, Y. Liu, H. Xin, Y. Zuo, Progressive damage analysis of PFRP double-lap bolted joints using explicit finite element method, *Compos. Struct.*, **152**, 860–869, 2016.
[26] Z. Hashin, Failure criteria for unidirectional fiber composites, *J. of Appl. Mech.*, **80**, 329–342, 1973.
[27] Y. Zhou, H. Yazdani-Nezhad, M. A. Mccarthy, et al., A study of intra-laminar damage in double-lap, multi-bolt, composite joints with variable clearance using continuum damage mechanics, *Compos. Struct.*, **116**, 441–452, 2014.
[28] R. M. O'Higgins, *An experimental and numerical study of damage initiation and growth in high strength glass and carbon fibre-reinforced composite materials*, phD. diss., University of Limerick, College of Engineering, Limerick, 2007.